Marin D, Fairlie M, Bunton P, Nwosu CN, Parker J, Franklin F, Novakovic K. [Design and validation study of a laboratory scale chemical reactor for non-invasive imaging of macro objects in situ](). ***Chemical Engineering Journal*** **2017**

Accepted Manuscript

Design and validation study of a laboratory scale chemical reactor for non-invasive imaging of macro objects in situ

Daniela Marin, Michael Fairlie, Patrick Bunton, Chinyelumndu Jennifer Nwosu, Julie Parker, Francis Franklin, Katarina Novakovic

PII: S1385-8947(17)31137-3
DOI: http://dx.doi.org/10.1016/j.cej.2017.07.001
Reference: CEJ 17266

To appear in: *Chemical Engineering Journal*

Received Date: 30 March 2017
Revised Date: 20 June 2017
Accepted Date: 1 July 2017

Please cite this article as: D. Marin, M. Fairlie, P. Bunton, C.J. Nwosu, J. Parker, F. Franklin, K. Novakovic, Design and validation study of a laboratory scale chemical reactor for non-invasive imaging of macro objects in situ, *Chemical Engineering Journal* (2017), doi: http://dx.doi.org/10.1016/j.cej.2017.07.001

Design and validation study of a laboratory scale chemical reactor for non-invasive imaging of macro objects in situ

Daniela Marin[a], Michael Fairlie[b], Patrick Bunton[a], Chinyelumndu Jennifer Nwosu[b], Julie Parker[b], Francis Franklin[c] and Katarina Novakovic*[b]

[a] Department of Physics, William Jewell College, Liberty, MO 64068, USA

[b] School of Chemical Engineering and Advanced Materials, Newcastle University, Newcastle, NE1 7RU, UK

[c] School of Mechanical and System Engineering, Newcastle University, Newcastle, NE1 7RU, UK

*Corresponding author: katarina.novakovic@ncl.ac.uk

Highlights

- A chemical reactor is designed for optical in situ imaging of macro objects
- Reactor design allows for agitation, probe mounting and temperature control
- Setup is evaluated by imaging a USAF 1951 resolution chart

- Setup is validated by imaging conformational changes in hydrogels over time
- Principles are applicable to any non-invasive imaging of a macro object in a reactor

Abstract

Inexpensive in situ monitoring of a conformational change in a macro object over long periods of time in a chemical reactor is challenging. One research area which would benefit from improvements in screening methods is the study of smart hydrogels, particularly when they are intended as oral forms for drug delivery or as multifunctional scaffolds replacing surgically removed tissues. Smart materials have the ability to alter their volume by swelling and/or collapsing in response to a specific stimulus in their environment. Conventional methods used to record this change such as gravimetric analysis, are invasive, require manpower for time-consuming hydrogel handling and often result in material fragmentation leading to inaccuracy. In this work, a novel reactor design is implemented in combination with inexpensive optics to achieve a non-invasive method that can be used reliably over long periods of time. Optical quality flat glass windows are incorporated in a jacketed reactor vessel design to

enable undistorted imaging. The reactor was made from a chemical engineering viewpoint to enable temperature control, continuous stirring and sampling while preventing evaporative loss of solvent. Image resolution was measured using a USAF 1951 resolution test target. The setup was validated using pH responsive PVP-Chitosan hydrogels to demonstrate the capabilities of the method in monitoring the change in volume of the responsive hydrogel with time.

Keywords: reactor design; optical reactor; in situ imaging; USAF 1951 chart; smart hydrogel;

Graphical abstract

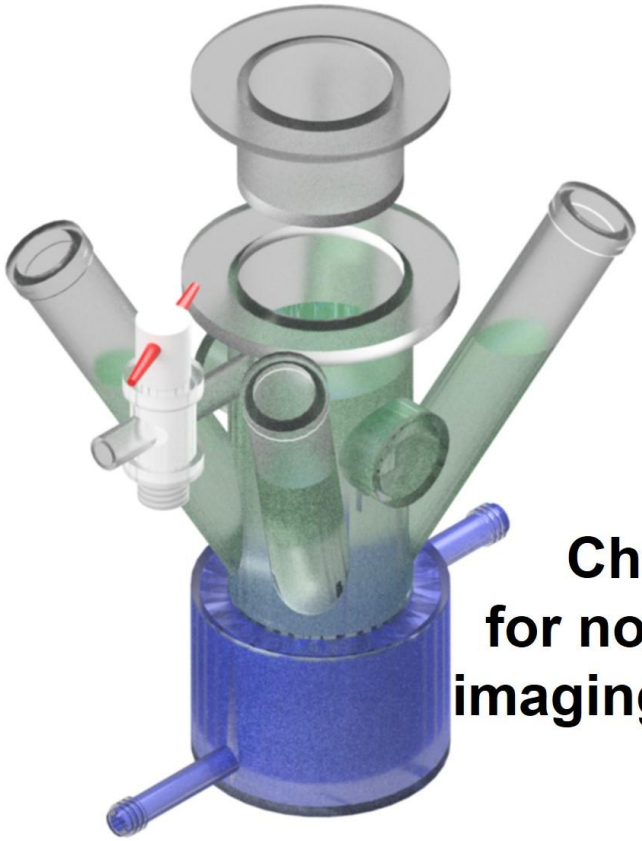

Chemical reactor for non-invasive in situ imaging of macro objects

1. Introduction

Chemical reactors are designed to optimise the chemical process taking place inside them. Temperature control, mixing and process monitoring are frequently required for process optimisation and control. In such cases the reactor incorporates a heating/cooling jacket, internal heater, stirrer and ports for sampling or probe mounting. The design of the chemical reactor must be capable of adapting as the requirements of the reaction system change.[1] The objective of this work is the design and validation of a lab-scale reactor for non-invasive in situ monitoring of changes in the size of a macro object over longer

periods of time, e.g. hours, days, weeks. This is particularly needed in the study of smart hydrogels. Smart hydrogels are soft materials that can reversibly respond to changes in a variety of chemical and/or physical stimuli in their environment by adjusting their conformation i.e. changing volume via swelling and de-swelling actions.[2], [3] These materials have attracted significant scientific interest since their discovery and are quickly progressing from proof of principle to applications in the areas of drug delivery, tissue engineering, biosensors, microfluidic devices and purification systems.[4], [5], [6], [7], [8], [9], [10], [11], [12], [13], [14] At all stages of development research, endeavours require measurements of conformational change, and various qualitative and quantitative methods have been pursued. Qualitative assessment is the reporting of general observations often accompanied by an example image of a sample.[15] Quantitative methods tend to report sample size (length, radius, and thickness) measured with a ruler or Vernier calliper, or the mass of a sample measured gravimetrically.[16], [17], [18] While all of these methods are useful, each has shortfalls. Visual observations are subjective, may be inconsistent and are difficult to compare between different laboratories. Measurement of size with rulers/callipers as well as gravimetrically requires sample handling which generates inaccuracy. Smart hydrogels predominantly consist of water and therefore have a soft structure. During the handling process some of this water may be lost and some fracturing or fragmentation of the hydrogel may occur, introducing errors in measurement. Furthermore, all of

these methods require human intervention and therefore are not ideal when lengthy monitoring periods are required.

In an attempt to resolve the aforementioned issues, optical methods have been introduced employing cameras and microscopes supported by digital image processing software.[15], [19], [20] While optical studies have led to progress in hydrogel imaging, in situ monitoring still faces limitations, in particular when lengthy screening in controlled conditions is needed. Additionally, samples are three-dimensional objects requiring imaging from multiple angles in order to reconstruct the actual size of the object and subsequent changes in size/volume. Also, containers used to store and study samples are typically made of curved glass which introduces image distortion when filled with a liquid.

This paper presents a lab-scale reactor which has been designed to enable the imaging of simple three dimensional objects over long periods of time in a controlled reaction environment. Various aspects of the prospective chemical processes were considered and the reactor was designed accordingly. A 1951 USAF resolution test target was used to test the resolving power of optical imaging while a pH responsive PVP-chitosan hydrogel was imaged as an example of an object whose change in volume requires screening over long periods of time.

2. Materials and Methods

2.1 Hydrogel Synthesis

Poly (vinyl pyrrolidone) (PVP) Mw 40,000 g/mol; chitosan (Cht) Mw 190,000–300,000 g/mol with 80% deacetylation; genipin (Gen) ≥98%; and glacial acetic acid were purchased from Sigma Aldrich. Glycine (pH 2) and phosphate (pH 7) buffers were obtained from Fisher Scientific. All chemicals were used as received. Cht was dissolved in an aqueous 1% (v/v) acetic acid solution with the aid of stirring at room temperature to attain a 1.5% (w/v) solution. A 5% (w/v) homogeneous transparent PVP solution was obtained by dissolving PVP in deionised water at room temperature. A transparent Gen solution 0.5% (w/v) was obtained by dissolving Gen powder in deionised water at room temperature. Two sets of hydrogel samples were prepared in polyethylene vials (Ø1 cm). The first combined 0.5 mL chitosan solution and 0.1 mL genipin solution with 0.5 mL PVP solution. The second combined 0.3 mL chitosan solution and 0.05 mL genipin solution with 0.1 mL PVP solution. In both cases mixtures were stirred for 5 min using a magnetic stirrer. Subsequently, the vials were closed and the samples polymerized at 37°C in an oven for 24 h. Following polymerization, samples were removed from the vials and stored in pH 7 buffer to contract prior to optical study.

2.2 Optical Experimentation

The optical studies reported employed the setup shown in Figure 1. The setup consists of a breadboard with mounts, a jacketed reactor especially designed for optical screening, two Nikon cameras (models 5100 and 7000) with AF-S Micro-Nikkor 105mm 1:2.8 G Nikon lenses, a water bath, a Pt100 temperature probe, a pH probe connected to a PC, additional lighting, and a magnetic stirrer. Note especially that a Nikon micro lens of comparatively long focal length was used (other manufactures term such a lens a macro lens). A micro lens is essential for resolving small features up close. While shorter focal length micro lenses are available at less expense, the longer focal length allows for additional freedom in the distance of the camera from the reactor. This lens, which is capable of 1 to 1 imaging, has a focal range of 0.314 m to infinity. On a DX format camera the maximum angular field of view is 15 degrees according to specifications from the manufacturer.

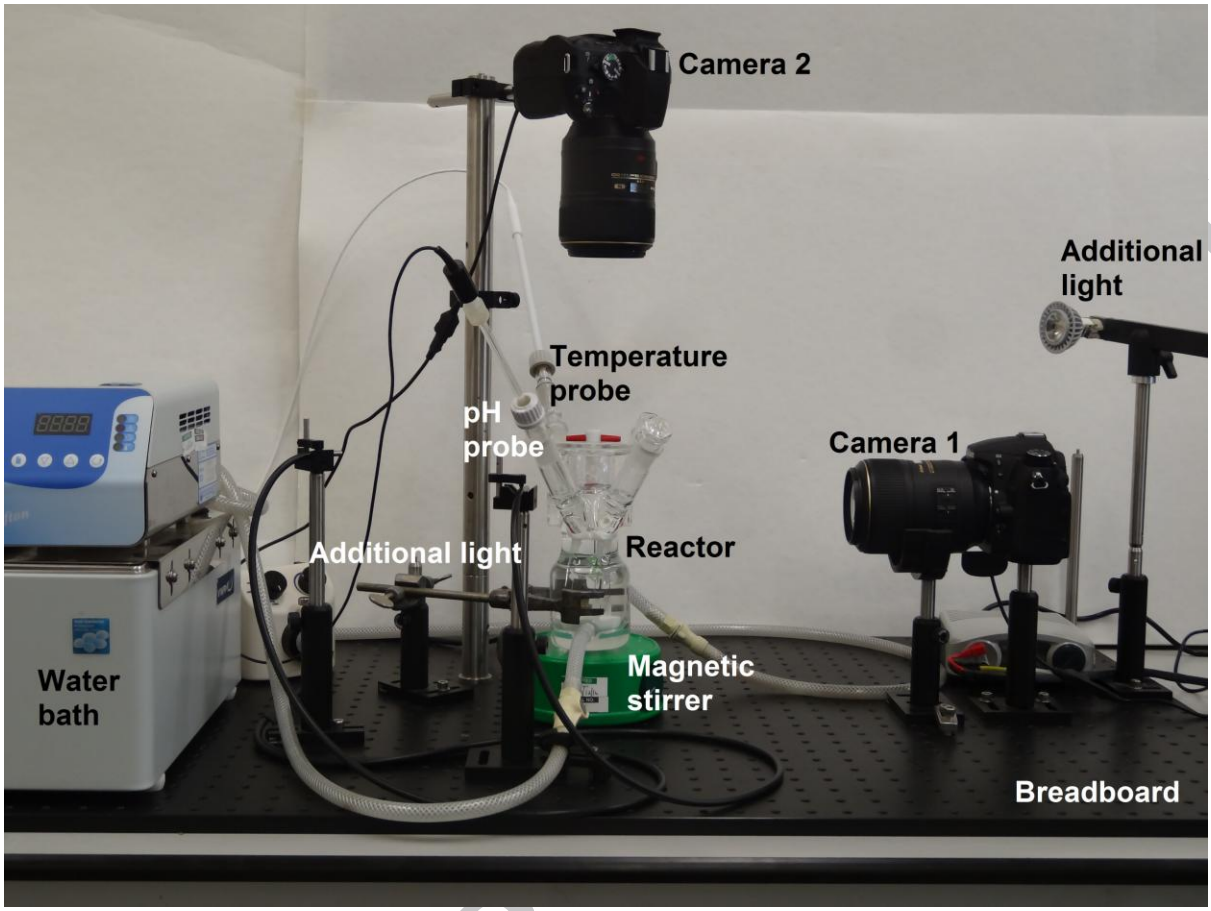

Figure 1 Experimental setup.

2.2.1 Optical Reactor Design

The reactor was designed (Figure 2) and manufactured in-house (Figure 3). To achieve a functional reactor vessel suitable for optical screening the following elements were incorporated in the design: two parallel windows on opposite sides of the reactor made form optical grade glass (Ø3 cm) for horizontal viewing; one window (Ø4 cm) made form optical grade glass incorporated in the reactor lid to enable vertical viewing; an inverted lid to allow the optical window to be immersed into the solution in the reactor to avoid issues with

condensation when operating the system over longer periods of time or when running the system at elevated temperatures; a reactor jacket so that temperature can be controlled; four ports for sampling and/or probe insertion; an overflow valve to enable continuous operation when such a configuration is required.

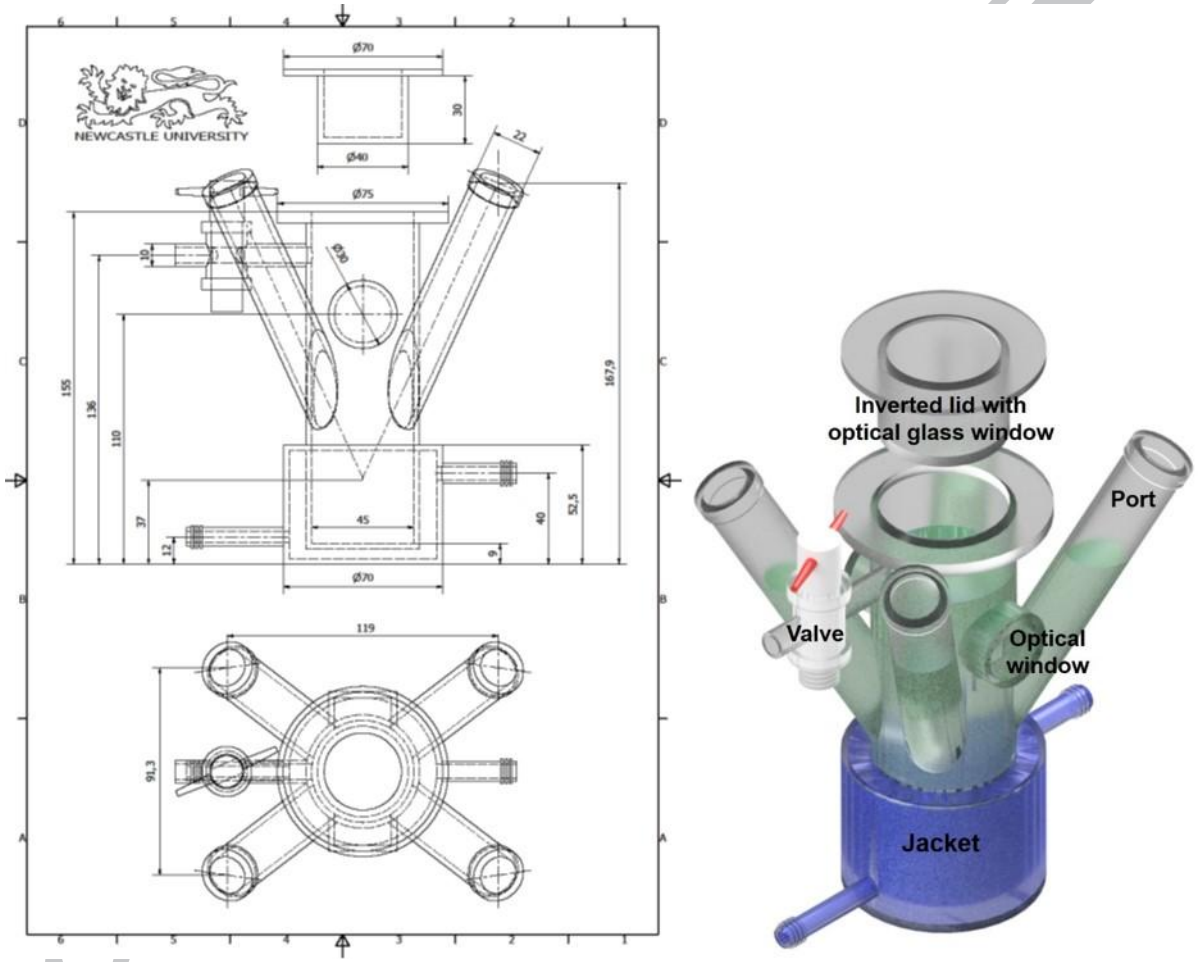

Figure 2 Optical reactor specifications.

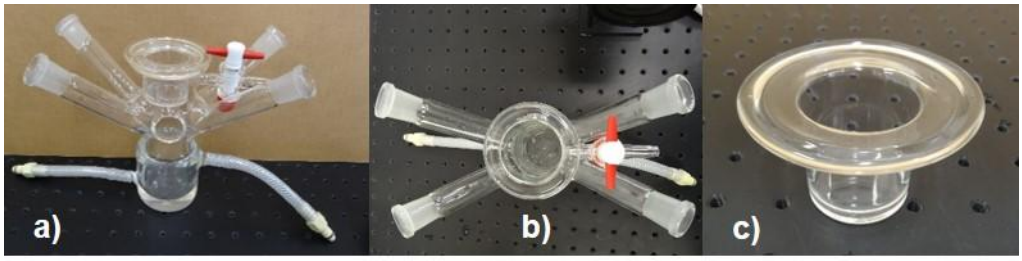

Figure 3 Optical reactor with lid: a) front view; b) top view; c) inverted lid.

2.2.2 Resolving Power of Optical Setup

The resolution of the imaging system was evaluated using the 1951 USAF resolution test target. The details of the USAF 1951 resolution chart can be found in the reference [21]. However, for practical purposes consult the catalogue of virtually any supplier of research-grade optics such as Thorlabs or Edmund Optics. This resolution test target (Figure 4a) consists of a number of pairs of three horizontal and three vertical lines ranging in size (Figure 4b). A single pair of horizontal and vertical lines is called an element (numbered from 1 to 6) with several elements forming a group (numbered from -2 to 9). When viewing an image, the two numbers corresponding with the smallest distinguishable line pair are noted and used to calculate resolution expressed as the number of line-pairs (lp) found in one millimetre (Equation 1).

$$\text{Resolution (lp/mm)} = 2^{\text{Group}+(\text{Element}-1)/6} \qquad \text{Equation 1}$$

For convenience, prepopulated tables defining the number of lp/mm as well as the width of a single line are also available (www.thorlabs.com).

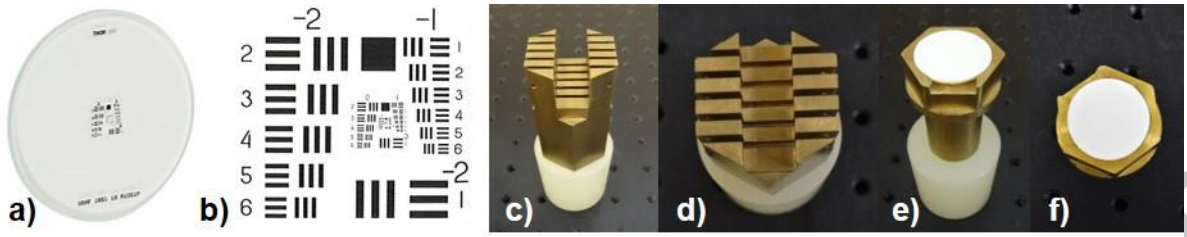

Figure 4 a) the 1951 USAF resolution test target (Ø25 mm); b) elements on the 1951 USAF resolution test target; c) front view of the stand for horizontal imaging of the resolution test target; d) top view of the stand for horizontal imaging of the resolution test target; e) front view of the stand for vertical imaging of the resolution target; f) top view of the stand for vertical imaging of the resolution test target.

Two stands, designed and manufactured in-house, were used to position the resolution test target in the reactor. The stand used to determine image resolution from the side (Figures 4c and d) incorporates five slots so that the resolution test target (Figure 4a) can be positioned vertically at different distances from Camera 1 (Figure 1) since the resolution achievable depends on this distance in conjunction with the f-number of the lens. Throughout this paper the slots are numbered from 1 (closest to Camera 1) to 5 (furthest from Camera 1). The second stand was used to resolve imaging from the top (Figure 4e and f) by supporting the resolution test target (Figure 4a) in a horizontal position for imaging using Camera 2 (Figure 1). The stands are used to evaluate the most effective resolution of the test target that can be applied to imaging of the macro object (hydrogel) changing in size over time in the reactor. This was

done by selecting the appropriate camera f-number setting (the ratio between the focal length and the aperture diameter). When the f-number of the lens is decreased, the resolution of the image increases, while the depth of field is reduced.[22] This means that for imaging macro scale samples, the resolution at the centre of the chamber must be reduced by selecting a higher f-number in favour of increased depth of field to maintain quality imaging throughout the extent of the sample.

The stand shown in Figure 4c was placed inside the jacketed reactor, which was filled with water. The resolution test target was placed in the middle slot (Slot 3) and the effect of a range of f-numbers on image resolution was studied using Camera 1. For each of the f-numbers the camera was focused on the resolution chart and an image was taken. Using the same settings without any further changes, the chart was moved to Slots 1 and 2 and images were taken for both positions. Slot 3 is used as a marker as it reflects the central crosscut of the hydrogel, a plane that remains unchanged. Slots 1 and 2 are used to mimic the gel swelling towards Camera 1. For imaging using Camera 2 (the top view), stand 4e was positioned inside the reactor and the resolution test target was placed on it. The f-number was set and an image was taken of the focused resolution test target. In all cases, images were evaluated for resolution using the 1951 USAF resolution test target table converter (www.thorlabs.com).

2.2.3 Evaluation of Image Distortion

To evaluate the improvement made by incorporating optical quality flat glass windows in the reactor design compared to a conventional curved vessel, image distortion was assessed. The setup consisted of a 25 by 25 mm piece of acrylic graph paper (mm scale) positioned in Slot 3 on the stand (Figure 4c) inside the optical reactor which was filled with water. Firstly, the graph paper was imaged through the optical windows following the methods described above. Following this, the stand was elevated to enable imaging through the curved surface of the reactor. The two images were compared using ImageJ software (http://rsbweb.nih.gov/ij/download.html) to assess the change in horizontal length between the graph lines 10 mm apart. Percent distortion was then calculated (Equation 2).

$$\text{Distortion } (\%) = \frac{\text{Curved glass distance} - \text{Optical flat glass distance}}{\text{Optical flat glass distance}} * 100$$

Equation 2

Where curved glass distance is the distance measured through the curved surface, and optical flat glass distance is the distance measured through the flat optical surface.

2.2.4 Evaluation of Condensation Effect

The effect of condensation on resolution was also assessed. The 1951 USAF resolution test target was positioned horizontally on the stand (Figure 4e) in the optical reactor which was filled with water and covered with either a flat glass lid or the inverted optical flat glass lid (Figure 2c). The inverted lid was immersed in the water. The water bath was programmed to maintain a temperature of 32 °C allowing the water in the reactor to be heated gently generating condensation. Images of the resolution test target were taken using Camera 2 with the optimized settings from the procedure described above (Section 2.2.2).

2.2.5 Optical Study of Hydrogels

As shown in Figure 1, the reactor was attached to a water bath set to the appropriate temperature. Temperature and pH probes connected to a data logging PC were inserted into two ports. The reactor was filled with buffer solution, and cameras were set using the optimised camera settings from Section 2.2.2. A hydrogel was positioned at the centre of the stand using a needle to hold the gel in place (Figure 5).To prevent the gel from floating, a small piece of PTFE was secured at the top of the needle leaving sufficient space for gel expansion. The stand and hydrogel were then lowered into the solution and imaging commenced. In the first experiment hydrogel swelling was monitored

in a pH 2 buffer solutions for 2 weeks, while in a second experiment pH 2 and pH 7 buffers were alternated every 24 h.

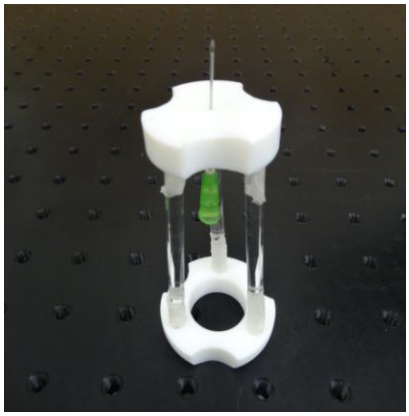

Figure 5 Stand used to position the hydrogel sample within the reactor, manufactured in-house.

The images obtained were viewed and analysed using ImageJ software. The height and top surface area of the hydrogels were quantified in arbitrary units (H_{arb} and A_{arb}) and the relative volumetric swelling ratio was calculated according to Equations 3-5. [15]

$$\Psi\,(\%) = \frac{V_{arb} - V_{0\,arb}}{V_{0\,arb}} * 100 \qquad \text{Equation 3}$$

$$V_{arb} = A_{arb} * H_{arb} \quad \text{Equation 4}$$

$$V_{0\,arb} = A_{0\,arb} * H_{0\,arb} \quad \text{Equation 5}$$

where Ψ is the relative volumetric swelling ratio; $V_{0\,arb}$ is the relative volume of the hydrogel at time zero; V_{arb} is the relative volume of the hydrogel at a given time after time zero; $A_{0\,arb}$ is the top surface area of the hydrogel measured at time zero; $H_{0\,arb}$ is the height (thickness) of the hydrogel measured at time zero; A_{arb} is the top surface area of the hydrogel after time zero; H_{arb} is the height (thickness) of the hydrogel measured after time zero.

As ImageJ produces arbitrary dimensions, a calibration is required to convert measurements to mm. Equations 6 and 7 demonstrate how the hydrogel height was calibrated.

$$H = x * H_{arb} \quad \text{Equation 6}$$

$$x = H_0 / H_{0\,arb} \quad \text{Equation 7}$$

Where H is the calibrated hydrogel height (mm); x is a calibration constant for height; H_{arb} is the arbitrary height given by ImageJ; H_0 is the known hydrogel height at time zero measured using a digital calliper (mm). A similar process was carried out for determining the hydrogel top surface area (Equations 8-10).

$$A = \pi * \left(\frac{y * d_{arb}}{2}\right)^2 \quad \text{Equation 8}$$

$$y = \frac{d_0}{d_{0\,arb}} \quad \text{Equation 9}$$

$$d_{arb} = \sqrt{\frac{A_{arb}}{\pi}} * 2 \quad \text{Equation 10}$$

Where A is the calibrated hydrogel top surface area (mm^2), y is a calibration constant for diameter; d_0 is the known hydrogel diameter measured at time zero

using the digital calliper (mm) while $d_{0\ arb}$ and d_{arb} are the arbitrary diameters calculated using ImageJ at time zero and afterwards; A_{arb} is the arbitrary top surface area given by ImageJ.

2.2.6 Evaluation of temperature and pH stability

To evaluate the effectiveness of the reactor jacket, the vessel was filled with pH 2 buffer and the water bath temperature was increased in 10°C steps from 25 to 75°C over approximately 3 days. Both temperature and pH were recorded inside the reactor at the position where the hydrogel sample would be situated.

3 Results and Discussion

Following the method outlined in Section 2.2.2, a range of f-numbers were evaluated using the horizontally mounted camera (Camera 1, Figure 1) along with the stand encompassing 5 slots (Figure 4c and d) and the USAF 1951 test target (Figure 4a). Once images were resolved for the middle slot (Slot 3), the same settings were used to image the USAF 1951 test target in Slots 1 and 2. The results are presented in Table 1.

Table 1 The effect of the f-number on resolution for Camera 1.

Slot #	f/#	Line pair/mm	Line width (μm)
3	19	20.16	24.80
2	19	8.98	55.68

1	19	5.04	99.21
3	22	16.00	31.25
2	22	11.31	44.19
1	22	6.35	78.75
3	27	16.00	31.25
2	27	14.25	35.08
1	27	8.98	55.68
3	32	14.25	35.08
2	32	14.25	35.08
1	32	10.08	49.61
3	38	10.08	49.61
2	38	10.08	49.61
1	38	11.31	44.19

As can be seen from Table 1, f-27 gave a low Slot 3 line width (31.25) and the second lowest average Slot 1-3 line width (40.67). Based on these results f-number 27 was selected for Camera 1 (Figure 1). Camera 2 (Figure 1) was assessed in a similar manner (Section 2.2.2) using the stand shown in Figure 4e and the USAF 1951 test target (Figure 4a). A horizontal sample height and corresponding focal plane was assessed and f/ 22 was found to give the best results. Example images of the USAF 1951 test target imaged using Cameras 1 and 2 are shown in Figure 6.

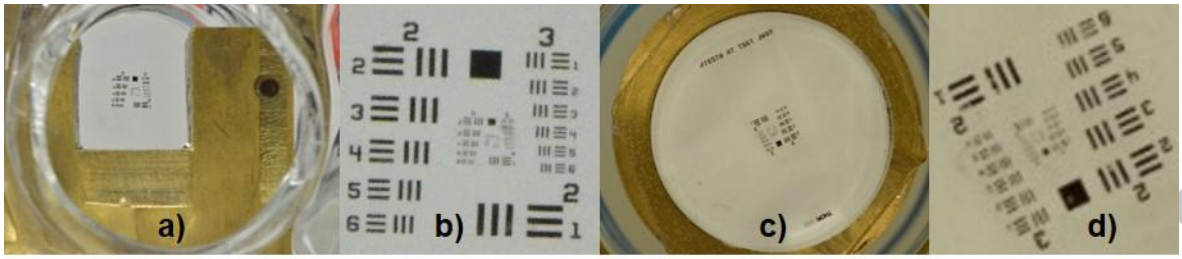

Figure 6 USAF 1951 test target images: a) Camera 1; b) Camera 1 magnified; c) Camera 2; d) Camera 2 magnified.

The same configuration was used to determine the effect of variation of magnification over the depth of field. Images of the resolution test target were taken in all five positions used above at f/27. ImageJ was used to compare a representative distance on the resolution test target across the five positions. Taking the central position (Slot 3) as a reference, the change in magnification varied from -2% for the position closest to the camera lens to just over +3% at the most distant position from the lens. Stated another way, there is a potential error of about +/-3 % over the depth of field of 40 mm. However, for the hydrogel measurements herein, the side edge of the round hydrogel sample, which remains at the Slot 3 position during swelling, was used to determine height so this error has no effect on the measured volumes.

The hydrogels were, therefore, imaged using Camera 1 set at f-number 27, exposure 1/10th s, ISO 2200 and Camera 2 set at f-number 22, exposure 1/10th s and ISO 2500. Higher ISO corresponds to increased sensitivity of the sensor

array while exposure (sometimes expressed as shutter speed) is the time the array is exposed to the light. The differences in ISO numbers between the two cameras are due to the variation in their specifications.

Image distortion was assessed to evaluate the improvement of incorporating optical quality flat glass windows in the reactor design compared to using a conventional curved vessel. It is recognized that imaging through curved glass introduces distortion. Simply put, distortion refers to variation in magnification over different parts of the image. This is particularly relevant when objects are viewed through a different medium where changes of refractive index distort the light seen.[23] In other words, the curved surface, in conjunction with the liquid medium contained within it, acts as an additional lens, which is generally undesirable. Using the method described in Section 2.2.3 and Equation 2, image distortion was calculated to be 32.7% when images were viewed using the curved vessel containing water rather than through the flat optical glass window. As can be noted from Figure 7, curved glass induces a so called "barrel" distortion. While a small level of distortion is associated with the camera lenses [24], it is clear that imaging through curved surfaces significantly reduces accuracy.

Figure 7 Imaging through a) curved glass; b) optical flat glass window. Image a) is magnified in the horizontal direction by the curved surface but not in the vertical.

The effect of condensation was captured following the method detailed in Section 2.2.4. Images captured using a flat glass lid and the immersed inverted lid (Figure 3c) are illustrated in Figure 8.

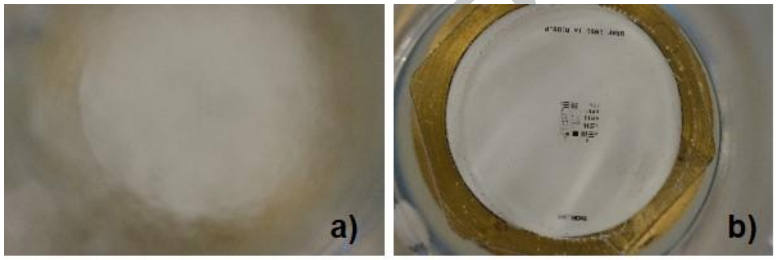

Figure 8 Effect of condensation: images captured via a) flat glass lid; b) inverted immersed lid.

To validate the reactor design and camera setup hydrogels prepared as detailed in Section 2.1 were imaged. The hydrogel with the increased amount of PVP (0.5 mL PVP) was imaged in pH 2 buffer at 20°C over two weeks to assess the durability of the setup. This hydrogel composition was selected as it swells significantly due to the increased PVP content which serves as a disintegrant

and thus enhances the increase in volume of the sample in addition to that which occurs from the tendency of chitosan to swell in acidic buffer.[15] Only images taken at the beginning and the end of the experiment are given in Figure 9. Using the ImageJ software and Equations 3-5 for the images shown in Figure 9 it was calculated that the hydrogel swelled 160%.

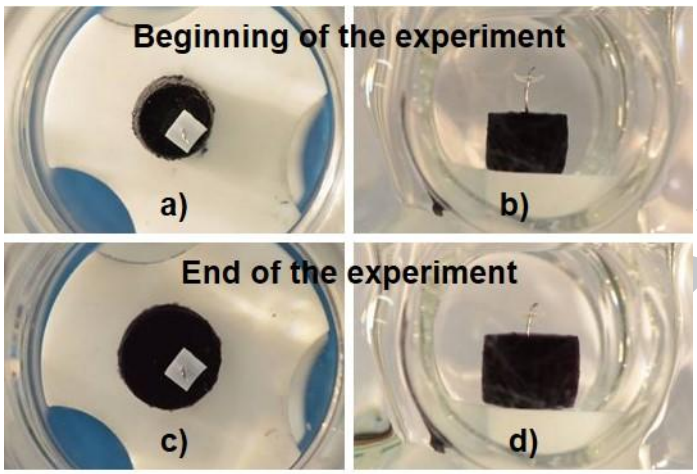

Figure 9 Hydrogel sample (0.5 mL chitosan, 0.1 mL genipin and 0.5 mL PVP solutions, polymerized at 37°C in an oven for 24 h and stored in pH 7 buffer to contract prior to optical study) imaged in pH 2 buffer over two weeks: a) beginning of the experiments: top view; b) beginning of the experiments: side view; c) end of the experiment: top view; d) end of the experiment: side view.

To illustrate the capabilities of the setup to record alternating pH environments, hydrogel samples with an increased amount of chitosan relative to PVP (Section 2.1) were imaged at 20°C in pH 2 buffer for 24 h followed by imaging in pH 7 buffer for another 24 h. Images were taken every 15 min. The sample composition was selected to ensure an increased responsiveness to pH change.

For that reason, the amount of chitosan was increased and the amount of PVP was decreased. Also, to achieve faster diffusion, thinner samples were synthesised. The experiment was repeated (Sample 1 and Sample 2) and results are given in Figure 10.

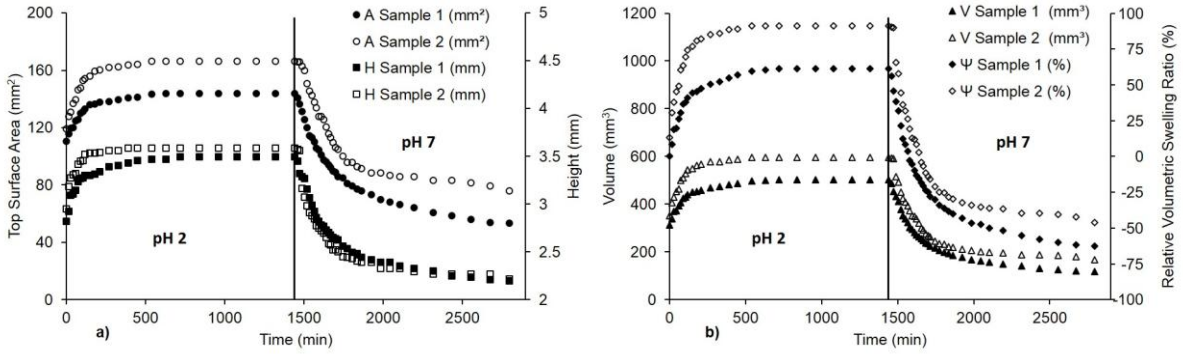

Figure 10 Change in size of hydrogel samples (0.3 mL chitosan, 0.05 mL genipin and 0.1 mL PVP solutions, polymerized at 37°C in an oven for 24 h and stored in pH 7 buffer to contract prior to optical study) imaged in alternating pH 2 and pH 7 buffers: a) top surface area (mm^2) and height (mm); b) hydrogel volume (mm^3) and relative volumetric swelling ratio (%).

As expected for chitosan based hydrogels, the hydrogel swells in an acidic environment (pH 2 buffer) and collapses in a basic (pH 7) environment. Figure 10 clearly shows that conformational changes in the gel can be successfully followed with time using this reactor setup. While a digital calliper was used to calibrate the size of the gel in these experiments other reference points are equally effective. For example, the height of the needle that positions the hydrogel is fixed and can be used as a reference point for the height of the gel

and the stand diameter can be used as a reference point for the top surface area of the gel.

The optical reactor was designed with a jacket to enable imaging at different temperatures. As the jacket only covers the lower section of the reactor a test was conducted to evaluate reactor performance at elevated temperatures. In the setup used, the water bath was set to the desired temperature while temperature and pH inside the reactor, which contained pH 2 buffer, were monitored using a Pt100 and a pH probe. The setup did not involve feedback and control of the water bath temperature in response to the temperature measured inside the reactor although this could be achieved with the necessary equipment.

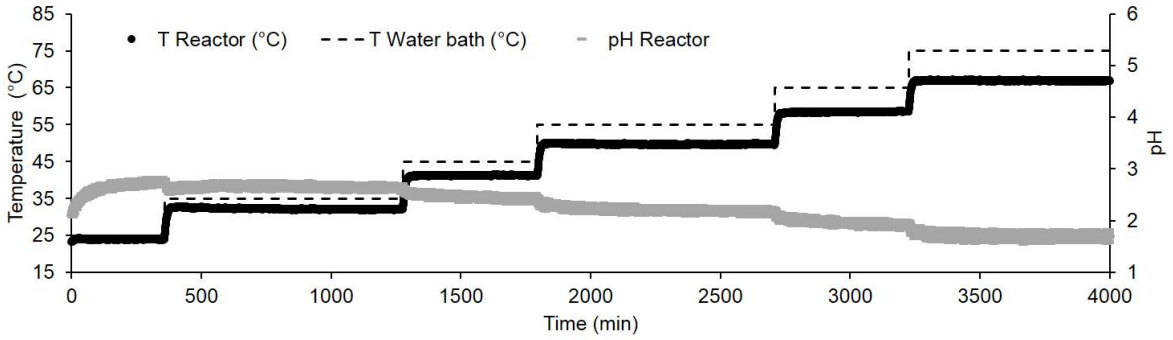

Figure 11 Temperature and pH recorded in a reactor filled with pH 2 buffer as water bath temperature was increased from 25 to 75°C in 10°C steps over approximately 3 days. Temperature and pH probes were positioned where the hydrogel sample would be situated.

As can be seen from Figure 11, a difference between the set and measured temperature exists which increases with the increase in operating temperature due to heat loss, however, the temperature inside the reactor is stable and constant at each set point. It can thus be concluded that, even in such a simple setup without feedback to regulate the water bath temperature in response to temperature inside the reactor, the desired temperature can be achieved by increasing the set point in the water bath. Equally, as pH is monitored rather than controlled, a pH decrease with an increase in set temperature is noted. This is expected as the formation of hydrogen ions is an endothermic process and with the increase in temperature the position of equilibrium shifts towards formation of hydrogen ions. [25]

In conclusion, a reactor suitable for non-invasive, in situ imaging of three-dimensional objects in a reactor over long time scales of the order of weeks has been designed and validated. The vessel is conceived in such a manner as to minimise image distortion, eliminate issues with condensation obstructing viewing, enable stirring, sampling, probe mounting and temperature control. Complementing the optical reactor, inexpensive optics are used making the proposed setup widely accessible. The resolving power of the system has been determined using a USAF 1951 resolution test target. The reliability of the method was demonstrated by screening hydrogel samples.

Acknowledgement

This work was supported by UK Engineering and Physical Sciences Research Council (EPSRC) grant numbers EP/H003908/1 and EP/N033655/1 and Newcastle University Visiting Professor Funding. DM gratefully acknowledges funding by a William Jewell College Journey Grant. PB acknowledges support by the National Science Foundation grant CBET-1335739. Authors wish to acknowledge the Newcastle University Glassblowing Service for manufacturing the reactors.

5. References

[1] H.S. Fogler, Elements of chemical reaction engineering, 2006.
[2] S. Chaterji, I.K. Kwon, K. Park, Smart polymeric gels: Redefining the limits of biomedical devices, Progress in Polymer Science, 32 (2007) 1083-1122.
[3] F. Liu, M.W. Urban, Recent advances and challenges in designing stimuli-responsive polymers, Progress in Polymer Science, 35 (2010) 3-23.
[4] S. Matcham, K. Novakovic, Fluorescence imaging in genipin crosslinked chitosan–poly(vinyl pyrrolidone) hydrogels, Polymers, 8 (2016) 385.
[5] A. Singh, N.A. Peppas, Hydrogels and scaffolds for immunomodulation, Advanced Materials, 26 (2014) 6530-6541.
[6] K. Tonsomboon, M.L. Oyen, Composite electrospun gelatin fiber-alginate gel scaffolds for mechanically robust tissue engineered cornea, Journal of the mechanical behavior of biomedical materials, 21 (2013) 185.
[7] N.A. Peppas, Devices based on intelligent biopolymers for oral protein delivery, International Journal of Pharmaceutics, 277 (2004) 11-17.
[8] G. Leone, 8 - Cartilage replacement implants using hydrogels A2 - Rimmer, Steve, in: Biomedical Hydrogels, Woodhead Publishing, 2011, pp. 149-183.
[9] A. Borzacchiello, A. Gloria, R. De Santis, L. Ambrosio, 6 - Spinal disc implants using hydrogels A2 - Rimmer, Steve, in: Biomedical Hydrogels, Woodhead Publishing, 2011, pp. 103-117.
[10] M.A. Reilly, K.E. Swindle-Reilly, N. Ravi, 7 - Hydrogels for intraocular lenses and other ophthalmic prostheses A2 - Rimmer, Steve, in: Biomedical Hydrogels, Woodhead Publishing, 2011, pp. 118-148.
[11] X. Feng, H. Wu, X. Sui, M.A. Hempenius, G. Julius Vancso, Thin film hydrogels from redox responsive poly(ferrocenylsilanes): Preparation,

properties, and applications in electrocatalysis, European Polymer Journal, 72 (2015) 535-542.
[12] Y. Liu, K. Zhang, J. Ma, G.J. Vancso, Thermoresponsive semi-IPN hydrogel microfibers from continuous fluidic processing with high elasticity and fast actuation, ACS Applied Materials & Interfaces, 9 (2017) 901-908.
[13] Y. Yajima, M. Yamada, E. Yamada, M. Iwase, M. Seki, Facile fabrication processes for hydrogel-based microfluidic devices made of natural biopolymers, Biomicrofluidics, 8 (2014) 024115.
[14] Y.-H. La, B. McCloskey, R. Sooriyakumaran, A. Vora, B. Freeman, M. Nassar, J. Hedrick, A. Nelson, R. Allen, Bifunctional hydrogel coatings for water purification membranes: Improved fouling resistance and antimicrobial activity, Journal of Membrane Science, 372 (2011) 285-291.
[15] C.J. Nwosu, G.A. Hurst, K. Novakovic, Genipin cross-linked chitosan-polyvinylpyrrolidone hydrogels: influence of composition and postsynthesis treatment on pH responsive behaviour, Advances in Materials Science and Engineering, 2015 (2015) 10.
[16] B.V. Slaughter, A.T. Blanchard, K.F. Maass, N.A. Peppas, Dynamic swelling behavior of interpenetrating polymer networks in response to temperature and pH, Journal of Applied Polymer Science, 132 (2015) n/a-n/a.
[17] J. Patterson, 10 - Imaging hydrogel implants in situ A2 - Rimmer, Steve, in: Biomedical Hydrogels, Woodhead Publishing, 2011, pp. 228-255.
[18] E. Kayalvizhy, P. Pazhanisamy, Swelling behavior of poly(N-cyclohexylacrylamide-co-acrylamide/AMPSNa) gold nanocomposite hydrogels, International Journal of Biological Macromolecules, 86 (2016) 721-727.
[19] G.A. Hurst, K. Novakovic, A facile in situ morphological characterization of smart genipin-crosslinked chitosan–poly(vinyl pyrrolidone) hydrogels, Journal of Materials Research, 28 (2013) 2401-2408.
[20] G.H. Darwish, H.H. Fakih, P. Karam, Temperature mapping in hydrogel matrices using unmodified digital camera, The Journal of Physical Chemistry B, 121 (2017) 1033-1040.
[21] E. Allen, S. Triantaphillidou, G.G. Attridge, R. Jenkins, S. Ray, E. Bilissi, The manual of photography and digital imaging, Routledge, 2010.
[22] L. Marshall, Basic closeup technique, Bee Culture, 133 (2005) 29-30.
[23] H. Haoxue, W. Lingling, T. Xiaoyong, L. Dichen, Y. Ming, W. Yu, Broadband gradient refractive index planar lens based on a compound liquid medium, Journal of Applied Physics, 112 (2012) 114913.
[24] T.-E. Kim, Analysis on the Characteristics of Camera Lens Distortion, Indian Journal of Science and Technology, 9 (2016).
[25] N.E. Good, G.D. Winget, W. Winter, T.N. Connolly, S. Izawa, R.M.M. Singh, Hydrogen ion buffers for biological research, Biochemistry, 5 (1966) 467-477.